AIAA Aviation
13-17 June 2016, Washington, D.C.
46th AIAA Fluid Dynamics Conference

DNS and PSE study on the stabilization effect of hypersonic boundary layer waves using 2-D surface roughness

Kahei Danny Fong[1] and Xiaolin Zhong[2]
University of California, Los Angeles, CA, 90095, USA

Recent studies have shown that roughness element can suppress mode S when it is placed at the right location. In particular, our previous DNS research has shown that when the 2-D roughness element is placed downstream of the synchronization location, mode S is suppressed. On the other hand, if the roughness element is located upstream of the synchronization point, mode S is amplified and destabilized. Recently, an experiment has confirmed the roughness stabilization effects on mode S by judiciously placing roughness elements downstream of the most dangerous frequency's synchronization point on a flared cone [1]. In the present paper, we extend our study on the roughness effect by using DNS and a theoretical approach of PSE analysis. The goals here are to investigate the mechanism of roughness effects observed in DNS simulations, and to study the role of neutral stability point and synchronization point. Different roughness heights and widths are considered similar to our previous studies [2]. It is found that PSE can indeed predict the roughness effects observed in DNS, and the PSE results confirm the trends of roughness height and width effects as seen in simulations. Our PSE results also suggest that the effect of roughness on Mack mode is the result of alteration of meanflow, and no new instability mode is found. Lastly, our DNS results overwhelmingly show that the synchronization location is an important parameter in determining the roughness effect comparing with the location of the neutral stability point.

I. Introduction

The physical mechanisms of the roughness induced boundary-layer transition are critical to the development of hypersonic vehicles. Transition can have a first-order impact on the lift and drag, stability and control, and heat transfer properties of the vehicles [3]. For example, roughness induced transition is an important consideration in the design of thermal protection systems (TPS) of hypersonic vehicles [4, 5]. For a reentry vehicle entering earth's atmosphere, it initially experiences a heating environment associated with a laminar boundary layer. As the vehicle altitude decreases, the vehicle surface becomes rougher and the boundary layer becomes turbulent. The transition from a laminar boundary layer to a turbulent one leads to the increase of surface heating rates by a factor of five or more. Thus the ability to understand and predict the physics of roughness induced transition plays an essential role in the design of TPS for reentry vehicles. Currently, roughness induced laminar-turbulent transition in hypersonic boundary layers, especially that induced by arbitrary surface roughness, is still poorly understood due to the limitation in experimental facilities and numerical methods [6].

Ideally the laminar-turbulent transition process can be divided into four stages. The first involves small disturbance fields which are initialized via a process termed "receptivity" by the viscous flow. The initial disturbance fields can involve both freestream and vehicle self-induced fluctuations such as acoustics, dynamic vortices, entropy spottiness, etc. The next stage is the linear growth stage, where small disturbances are amplified until they reach certain amplitude where nonlinear effects become important. The amplification can be in the form of exponential growth of eigenmodes (Tollmien-Schlichting waves or Mack waves) and non-modal growth of optimal disturbances (Transient growth). Once a disturbance has reached a finite amplitude, it often saturates and transforms the flow into a new, possibly unsteady state, which is termed as the secondary instability stage. The last stage is the breakdown stage where nonlinearities and/or high-order instabilities excite an increasing number of scales and frequencies in the flow.

[1] Graduate Research Assistant, Mechanical and Aerospace Engineering Department.
[2] Professor, Mechanical and Aerospace Engineering Department, AIAA associate fellow.

The receptivity study is mainly concerned with the excitation of instability waves, the characteristics of which can be analyzed by the linear stability theory (LST) [7]. The LST analyzes the propagation of individual sinusoidal waves in the streamwise direction inside the boundary layer. These waves are referred as Tollmien-Schlichting (T-S) waves for low speed flow, whose amplitudes vary though the boundary layer and die off exponentially outside the boundary layer. Extensive numerical and theoretical researches have been conducted to solve the linearized Navier-Stokes equations and many characteristics regarding the instability waves in hypersonic boundary layers have been discovered [7-11]. Mack [7] identified the unstable modes by using the LST for compressible flow. He showed that inside a supersonic boundary layer, there are multiple higher instability modes in addition to the first mode, which is the compressible counterpart of T-S waves in the incompressible boundary layers. These instability modes in the supersonic boundary layer are termed as first mode, second mode, third mode, etc. For supersonic boundary layer with Mach number larger than four, Mack's second mode is the most unstable mode, and it plays an important role in hypersonic boundary layer transition.

Direct numerical simulation has become an effective research tool for studying hypersonic boundary layer receptivity, stability, and transition by numerically solving the time-dependent three-dimensional Navier–Stokes equations for the temporally or spatially evolving instability waves. Malik et al. [12] investigated the responses of a Mach 8 flow over a sharp wedge of a half-angle of 5.3^o to three types of external forcing: a planar freestream acoustic wave, a narrow acoustic beam enforced on the bow shock near the leading edge, and a blowing-suction slot on the wedge surface. They concluded that these three types of forcing eventually resulted in the same type of instability waves in the boundary layer. Ma and Zhong [13] studied the receptivity mechanisms of the same hypersonic boundary layer to various freestream disturbances, i.e., fast and slow acoustic waves, vorticity waves, and entropy waves, by solving the two-dimensional compressible Navier-Stokes equations. They found that the stable modes in the boundary layer played a very important role in the receptivity process. Recently, Wang et al. [14] further studied the response of the Mach 8 flow over a 5.3^o half-angle sharp wedge to wall blowing–suction. The results showed that mode S is strongly excited when the actuator is located upstream of the corresponding synchronization point. There is no significant amplification of pressure perturbation when the actuator is downstream of the synchronization point. Although the exact cause and mechanism of this result were not clear, such a result was obtained for wall blowing–suction at all frequencies considered in their study.

Balakumar [15] numerically investigated the receptivity of a 2-D roughness to acoustic waves and found the isolated roughness does not contribute much in generating unstable disturbances. Marxen et al. [16] simulated the effects of a localized two-dimensional roughness element on the disturbance amplification in a hypersonic boundary layer. Their numerical experiments showed that in the vicinity of the separation regions, which are located in the upstream and downstream of the roughness, an increased amplification of a second-mode disturbance occurs for a certain frequency. Marxen et al. [17] studied the disturbance growth on a flat-plate boundary layer at Mach 4.8 with localized 2-D roughness element. They found the disturbance was strongly damped downstream of the roughness element around the separation region, which agrees with Holloway's hypothesis. However, the mechanisms were not investigated. At the same time, Duan et al. [18] from Zhong's group at UCLA reported that a 2-D roughness element can damp disturbances if the element is placed downstream of the synchronization location. The details of the work by the UCLA group will be discussed in the next paragraph. Riley et al. [19, 20] also numerically studied the stability characteristics of a Mach 4 hypersonic boundary layer over a wedge. On the surface of the wedge, they imposed convex or concave panel buckling (compliant panel) at different locations. They found that when the panel is placed near the trailing edge of the wedge, the panel can move the boundary layer transition further downstream. On the other hand, Egorov, Novikov and Fedorov [21] performed numerical simulations of a Mach 6 supersonic boundary layer over a grooved wavy plate. Their study was motivated by the numerical studies of Balakumar [22] and Egorov et al. [23] which showed the second mode remains neutral in the separated region on a 5.5 deg compression corner. Based on the result on the separated region, the intention of the study by Egorov et al. was to generate short local boundary layer separations by the wavy wall to decrease disturbance growth. The wavy wall was in the form of 9 round arc cavities. It was found that the wavy wall design damps a range of high frequency unstable disturbances which are relevant to the second mode instability. Bountin et al. [24] later confirmed the results in Egorov et al. [21] that the wavy wall damps the unstable second mode in the high frequency band while it enhances them at lower frequencies. Their experimental data also showed that the wavy wall damps disturbances not only at the wavy wall wavelength, but also a wide range of disturbances in different frequencies with different wavelengths. Based on these results, they argued that the stabilization effect of second mode by the wavy wall is due to altering the mean flow instead of an interference process between the second mode and the wavy wall itself.

Since 2009, for the purpose of simulating hypersonic flow with finite height roughness element, Zhong's group at UCLA has developed a high-order cut-cell method [25]. The new method was then applied to simulating a finite roughness elements on a hypersonic boundary layer at Mach 5.92 [18, 25]. Different from the wavy wall idea as in [26] and [21], they found that the relative location of 2-D roughness element and synchronization location plays an important role. Duan et al.[18] and Fong et al. [27] argue that 2-D roughness elements can damp disturbances if the roughness element with a height less than the local boundary layer thickness are downstream of the synchronization point. A further parametric study was performed by Fong et al. [28], in which different roughness parameters including roughness height, width and spacing between roughness elements have been considered. All results are consistent with the initial finding about the important of the synchronization location and roughness element location. On the other hand, despite the parallel flow assumption taken by LST, it has been shown in [29] that LST is capable of predicting the roughness effect observed in simulations. To extend this study, in this paper, both DNS and theoretical analysis using parabolized stability equation (PSE) are utilized. The DNS code is a high order shock fitting method combined with the high order cut cell method as described in [25]. On the other hand, PSE code is developed following the work by Gao et al.[30], Chang et al. [31] and Park et al.[32]. The goals of the present study are to investigate the mechanism of roughness effect using both DNS and PSE, and to study the importance of neutral stability point and the synchronization point. It is found that PSE can indeed predict the roughness effects observed in DNS, and the PSE results confirm the trends of roughness height and width effects seen in our simulations [2]. Our PSE results also suggest that the effect of roughness on Mack mode is the result of alteration of meanflow, and no new instability mode is found in PSE. Lastly, our DNS results overwhelmingly show that the synchronization location has an important role in determining the roughness effect comparing with the location of the neutral stability point.

II. DNS method

A schematic of a computational domain and a cut-cell grid in roughness induced hypersonic boundary layer transition is shown in Figure 1. This figure shows a typical hypersonic flow over a blunt body, where a bow shock is created by the supersonic freestream. In this paper, a high-order shock-fitting method is used to track the movement of the bow shock which is treated as the upper boundary of the computational domain. The computational grid for a shock-fitting formulation is bounded between the bow shock above and the blunt body below. The cut-cell grid is a smooth curvilinear grid fitted to the baseline body shape without the roughness. As a result, the roughness surface cuts across the grid lines. The roughness surface, Γ, is represented by surface equation in the following form,

$$\Gamma : f(x, y, z) = 0 \tag{1}$$

For a problem concerning practical arbitrary roughness, it is likely that there is no analytical equation applicable to represent the shape of the roughness element. In this case, a set of n discrete points $\{(x_1, y_1, z_1), (x_2, y_2, z_2), ..., (x_n, y_n, z_n)\}$ are used to represent the surface.

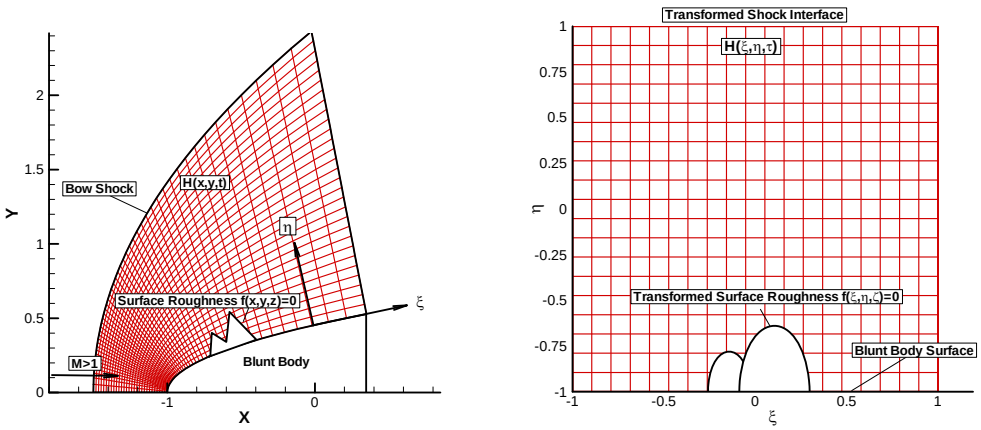

(a) **(b)**

Figure 1.Physical and computational domain and a cut-cell grid of hypersonic flow over a blunt body with surface roughness: a) physical grid, b) computational grid with a transformed roughness [19].

The roughness equation (1) in the physical domain is transformed into a Cartesian computational domain bounded by bow shock and flat plate. Under the computational coordinate system, the body fitted grids are represented by a curvilinear three-dimensional coordinates (ξ,η,ς) along the grid lines. The unsteady movement of the bow shock is treated as the computational upper boundary located at $\eta=\eta_{\max}$, which is time dependent. The other grid lines $\xi=const$ and $\varsigma=const$ remains stationary during computations. The coordinate transformation is defined by:

$$\begin{cases}\xi=\xi(x,y,z)\\ \eta=\eta(x,y,z,t)\\ \varsigma=\varsigma(x,y,z)\\ \tau=t\end{cases}\leftrightarrow\begin{cases}x=x(\xi,\eta,\varsigma,\tau)\\ y=y(\xi,\eta,\varsigma,\tau)\\ z=z(\xi,\eta,\varsigma,\tau)\\ t=\tau\end{cases} \tag{2}$$

where (x,y,z,t) are the physical coordinates defined under Cartesian coordinate system.

A third-order accurate Cut-Cell method is used in current numerical simulation [18]. A set of uniformly distributed Cartesian grids can be generated in the computational domain where the grid distribution in the physical domain is not uniformly distributed. Because smooth body-fitted grids are generated in the regular computational domain without the roughness, some of the Cartesian grid cells may be cut by the roughness boundary, which leads to irregular Cartesian grid cells. More details of the grid structure are discussed in a previous paper [18].

III. Parabolized Stability Equation

Linear stability analysis (LST) has been widely used to study stability characteristics of hypersonic boundary layer flow. One major assumption of LST is the parallel flow assumption, which ignores boundary layer growth. Although LST is usually accurate for analysis on hypersonic boundary layer on a smooth surface, in the case of our study of roughness effects, parallel flow may not be adequate.. Thus, the method which allows slow boundary layer growth, the parabolized stability equation (PSE) analysis, is considered here. The derivation of PSE is derived in a similar manner as the LST. However, in PSE, the wall normal velocity component *v* is kept in the governing equations. The three dimensional Navier-Stokes equations used in PSE for the perfect gas are,

$$\rho^*[\frac{\partial u^*}{\partial t^*}+u^*\cdot\nabla u^*]=-\nabla p^*+\nabla\cdot[\lambda^*(\nabla\cdot u^*)I+\mu^*(\nabla u^*+\nabla u^{*\mathrm{tr}})] \tag{3}$$

$$\frac{\partial\rho^*}{\partial t^*}+\nabla\cdot(\rho^* u^*)=0 \tag{4}$$

$$\rho^* c_p^*[\frac{\partial T^*}{\partial t^*}+u^*\cdot\nabla T^*]=\nabla\cdot(k^*\nabla T^*)+\frac{\partial p^*}{\partial t^*}+u^*\cdot\nabla u^*+\phi^* \tag{5}$$

$$p^*=\rho^* R^* T^* \tag{6}$$

where u^* is the velocity vector, ρ^* is the density, p^* is the pressure, T^* is the temperature, R^* is the gas constant, c_p^* is the specific heat at constant pressure, k^* is the thermal conductivity, μ^* is the first coefficient of viscosity, and λ^* is the second coefficient of viscosity. The viscous dissipation function, Φ^* is given as

$$\Phi^*=\lambda^*(\nabla\cdot u^*)^2+\frac{\mu^*}{2}(\nabla\mu^*+\nabla\mu^{*\mathrm{tr}}) \tag{7}$$

The superscript * represents dimensional quantities. In the PSE analysis, the quantities in the governing equations are non-dimensionalized by the freestream quantities similar to those in LST analysis. On the other hand, the instantaneous non-dimensional values of velocities, u,v,w, pressure p, temperature T, density ρ may be represented as the sum of mean and fluctuation quantity, i.e.

$$
\begin{aligned}
&u = \bar{U} + \tilde{u},\ \mathrm{v} = \bar{V} + \tilde{v}, \mathrm{w} = W + \tilde{w} \\
&p = \bar{P} + \tilde{p}, \mathrm{T} = \bar{T} + \tilde{T}, \rho = \bar{\rho} + \tilde{\rho} \\
&\mu = \bar{\mu} + \tilde{\mu}, \lambda = \bar{\lambda} + \tilde{\lambda}, k = \bar{k} + \tilde{k}
\end{aligned} \tag{8}
$$

Substitute Eqn. (8) into the non-dimensional form of governing equations yields the linearized full perturbation equation,

$$
\begin{aligned}
&\Gamma \frac{\partial \phi}{\partial t} + A\frac{\partial \phi}{\partial x} + B\frac{\partial \phi}{\partial y} + C\frac{\partial \phi}{\partial z} + D\phi = \\
&V_{xx}\frac{\partial^2 \phi}{\partial x^2} + V_{yy}\frac{\partial^2 \phi}{\partial y^2} + V_{zz}\frac{\partial^2 \phi}{\partial z^2} + V_{yz}\frac{\partial^2 \phi}{\partial y \partial z} + V_{xz}\frac{\partial^2 \phi}{\partial x \partial z} + V_{xy}\frac{\partial^2 \phi}{\partial x \partial y}
\end{aligned} \tag{9}
$$

where ϕ contains the perturbation vector and is defined as $\phi = [\tilde{p}, \tilde{u}, \tilde{v}, \tilde{w}, \tilde{\mathrm{T}}]^T$, and the coefficient matrices are composed of the meanflow quantities.

Different from the LST, in 2D PSE, the normal node of a perturbation is assumed to have the following form,

$$
\phi(x, y, z, t) = \psi(x, y) \exp(\mathrm{i} \int_{x_0}^{x} \alpha dx + \beta z - \omega t) \tag{10}
$$

where $\psi(x, y)$ is defined as the shape function as $\psi = [\hat{p}, \hat{u}, \hat{v}, \hat{w}, \hat{T}]^T$ similar to $\hat{q}(y_n)$ in the LST. In PSE, the streamwise wave number α is a function of x . On the other hand, the perturbation eigenfunction ψ is a function of both x and y instead of pure function of y in the LST analysis. Substituting Eqn. (10) into Eqn. (9), neglecting all terms which are of order of $1/R_0^2$, we obtain,

$$
\tilde{A}\frac{\partial \psi}{\partial x} + \tilde{B}\frac{\partial \psi}{\partial y} + \tilde{D}\psi = \tilde{V}_{yy}\frac{\partial^2 \psi}{\partial y^2} \tag{11}
$$

where

$$
\begin{aligned}
&\tilde{A} = \bar{A} - 2i\alpha\bar{V}_{xx} - i\beta\bar{V}_{xz} \\
&\tilde{B} = \bar{B} - i\alpha\bar{V}_{xy} - i\beta\bar{V}_{yz} \\
&\tilde{D} = -i\omega\bar{\Gamma} + i\alpha\bar{A} + i\beta\bar{C} + \bar{D} + \bar{V}_{xx}\alpha^2 + \bar{V}_{xz}\alpha\beta + \bar{V}_{yy}\beta^2 - i\bar{V}_{xx}\frac{d\alpha}{dx} \\
&\tilde{V}_{yy} = \bar{V}_{yy}
\end{aligned} \tag{12}
$$

Eqn. (12) is solved using finite difference scheme. The determining factor in choosing the streamwise marching scheme is stability. Thus, a simple backward Euler method is used for marching in the x -direction. A three points finite difference scheme is used in the wall-normal direction y . On the wall, two points finite difference scheme is adopted. In solving the PSE, it is noted that PSE is nonlinear because the coefficients include the unknown quantity α . Consequently, an iterative procedure for α is given as follows,

$$
\alpha^n = \alpha^{n-1} - i[\int_0^\infty \hat{q}_n \frac{\partial \hat{q}_n}{\partial x} dy / \int_0^\infty |\hat{q}_n|^2 dy] \tag{13}
$$

where $\hat{q}_n = (\hat{u}, \hat{v}, \hat{w})$, the superscript n and n-1 indicate the new value and old value. Eqn. (13) is equivalent to saying that the perturbation kinetic energy remains constant along the streamwise direction. Malik [33] has shown that this iterative procedure is a satisfactory approach for computing α .

IV. Results and Discussions

A. Previous Results

It has been shown in Fong et al. [29] that roughness element placed downstream of synchronization point can damp perturbations. Figure 2 shows the perturbation frequency spectrum obtained from DNS at locations downstream of roughness. For comparison, a case without roughness is included and shows on the right figure. The roughness location corresponds to the synchronization point for perturbation at frequency 133.26 kHz which is highlightened in the figure. It can be clearly seen that for perturbations at frequencies lower than 133.26 kHz, they are amplified by the roughness element. On the other hand, perturbations at frequencies higher than 133.26 kHz are damped by the roughness. Since it is known that the synchronization locations for high frequencies are more upstream, the roughness element therefore is located downstream of the synchronization locations for frequencies higher than 133.26 kHz. Vice versa, the synchronization locations for low frequencies are more downstream, the roughness element is therefore upstream of the synchronization locations for frequencies higher than 133.26 kHz. This relation between synchronization location and roughness element is the major finding in our previous DNS efforts [2, 27, 29, 34, 35].

To see if this damping/amplification effect observed in DNS can be predicted using an theoretical approach, LST analysis has been performed in [29] at a location downstream of roughness element. Figure 3 shows the wave number and growth rate spectrum (dimensional growth rate where positive is unstable) for roughness case and no roughness case obtained from LST. It is seen that the roughness element does not have a significant impact on wave number. However, its effect on growth rate is significant. The lines of growth rate for roughness case and no roughness case intercept at almost exactly at the synchronization frequency 133.26 kHz, which shows the importance of the synchronization frequency. It can also be seen that for frequencies higher than 133.26 kHz, the growth rate is lower for roughness case while for frequencies lower than 133.26 kHz, the growth rate is higher. This result from LST analysis is consistent with what have been observed in DNS.

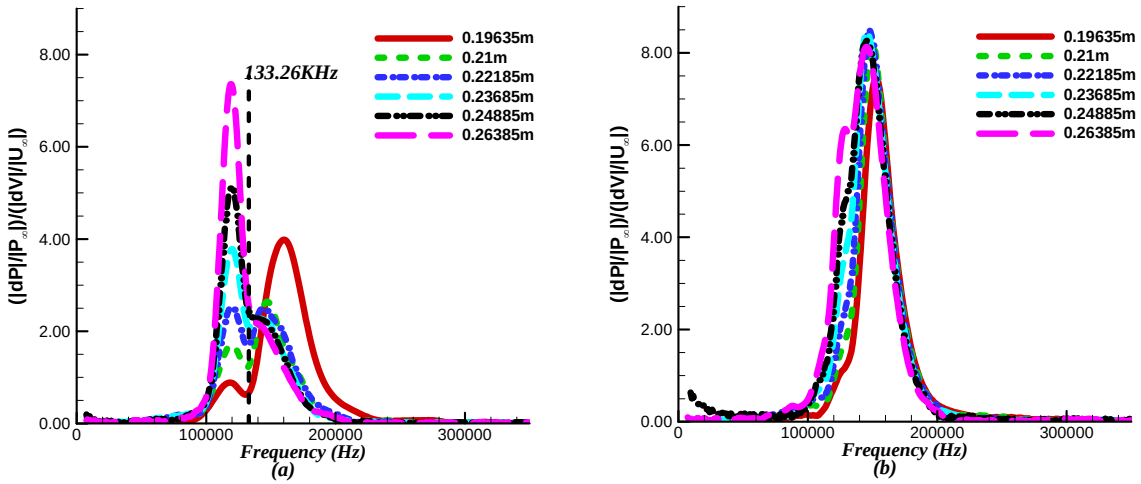

Figure 2. Non-dimensional frequency spectra of wall pressure perturbation at different location. (a) Downstream of roughness (b) No roughness case

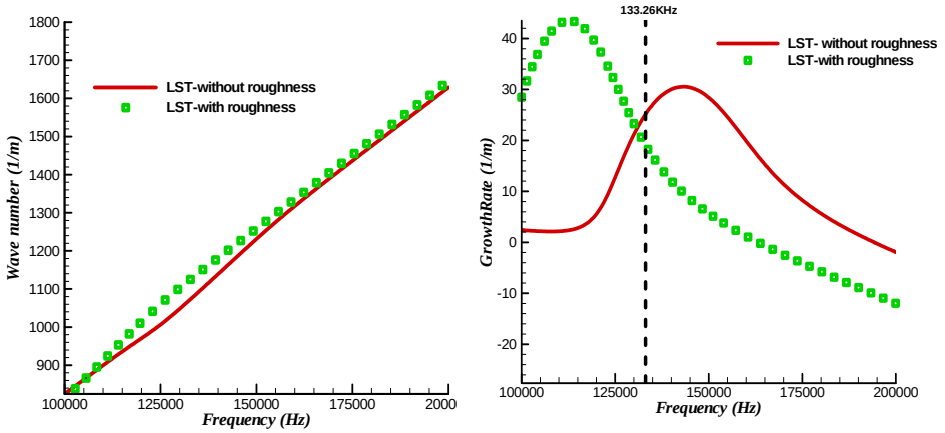

(a) **(b)**

Figure 3. LST prediction of wave number and growth rate for meanflow with roughness and without roughness at $x = 0.17385m$ **.**

B. Validation of PSE Code

In this present paper, PSE is used to fulfill the interest of seeing how non-parallel effects impact the results observed in DNS shown in [2, 27], and how important is non-parallel effect on the predication of roughness effects compared to LST. The PSE analysis enables the study of the evolution of discrete mode in a non-parallel flow condition with roughness elements. Since this method considers non-parallel effect, it allows one to study and compare numerical results with a better physical insight.

The first step of the PSE study involves its validation by reducing the PSE code to LST analysis for the Mach 5.92 flow without roughness element. The validation is done by assuming parallel flow (ex: taking any d/dx and high order derivatives in streamwise direction as zeros, and setting wall normal velocity v as zero) in PSE, and check if the results match with those predicted by the original LST code. Figure 4 (a) shows the growth rate obtained from PSE with parallel flow assumption comparing with the LST results for 100 kHz perturbation along the streamwise direction. Note that in the figure, the growth rate is the imaginary part of α in eqn.(10), which is non-dimensional. In this definition, the mode is unstable if the non-dimensional growth rate is negative. It can been seen that the result of PSE agree with LST very well, and are almost on top of each other despite the two results are generated by two completely separated codes. Figure 4 (b) shows good agreement between PSE and LST in phase velocity for perturbation at 100 kHz. Both Figure 4 (a) and (b) suggest the PSE code can be reduced to LST correctly, thus our PSE code is validated.

Next, the growth rate obtained from LST and PSE are compared with the actual DNS data as shown in Figure 5. In the figure, 150 kHz perturbation is chosen because this frequency is the most unstable in this location range in the DNS data. As it can be seen in the figure, both PSE and LST can resolve the unstable range reasonably well; however, comparing PSE with LST, PSE can capture the growth rate closer to the DNS data. For example, starting from the location at x=0.18 m, the LST result is moving away from the DNS data, while on the other hand, the PSE result still follows the DNS data in this location range. Figure 6 shows the eigenvector or the mode shape of perturbation at 150 kHz taken at a location of x=0.192 m. It is seen that in the wall region (non-dimensional coordinate in wall normal direction of Y/L < 10), the result of DNS, PSE and LST almost overlap with each other. However, in the region of 10 < Y/L < 30, the high gradient part of the mode shape cannot be resolved nicely with LST, while PSE is still capable of matching the DNS data accurately this region. Away from the wall, the LST and PSE results collapse with the DNS data again. From Figure 4 and Figure 6, it can be seen that although LST is typically sufficient for stability analysis of boundary layer flow, but PSE gives an even more accurate predication than LST.

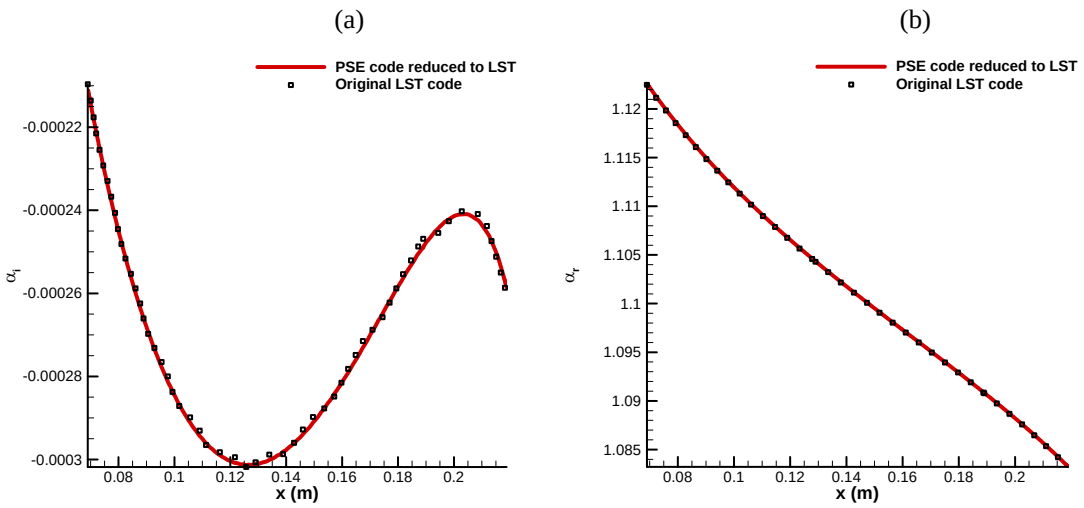

Figure 4. (a) Growth rate (b) Phase velocity obtained from LST and PSE for 100 kHz perturbation.

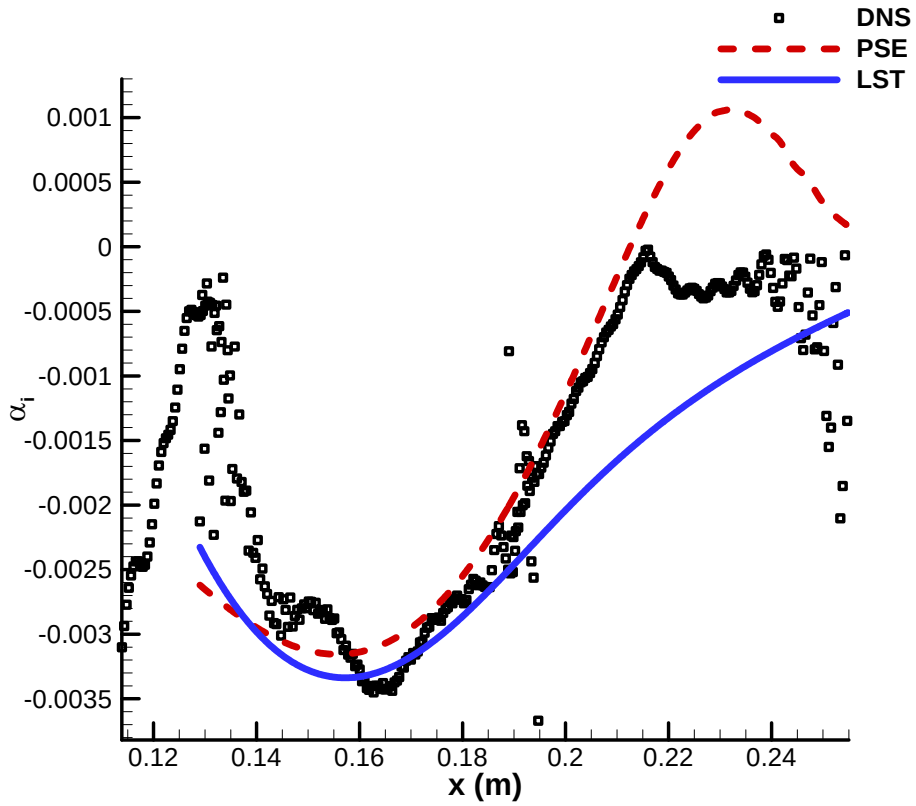

Figure 5. Comparison of growth rate obtained from DNS, PSE and LST at 150 kHz.

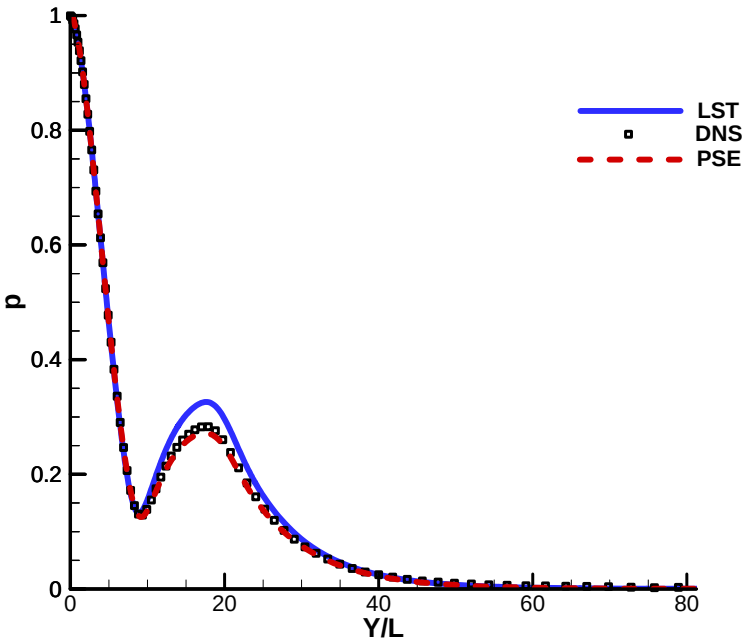

Figure 6. Comparison of mode shape obtained from DNS, PSE and LST at 150 kHz at x=0.192m.

C. Roughness Effect by PSE

After the validation, the PSE code is applied to the meanflow with roughness elements. The objective here is to use PSE to analyze the meanflow altered by roughness element and see if the damping effect observed in DNS can also be predicted by PSE. The case used here is the same meanflow as the one mentioned in [36]. For instance, the flow condition is,

$$\begin{cases} P_r = 0.72, R_\infty = \rho_\infty u_\infty / \mu_\infty = 13.2\times 10^6 / m \\ M_\infty = 5.92, T_\infty = 48.69K, P_\infty = 742.76Pa, T_w = 334.9K \end{cases}$$

The roughness is located at x = 0.185 m. This roughness location responds to the synchronization frequency of perturbation at 133.26 kHz. Based on previous DNS data, roughness can damp perturbations higher than the synchronization frequency while it amplifies the perturbations lower than the synchronization frequency. Figure 7 and Figure 8 show the growth rate predicted by PSE for two different roughness heights (50% and 10% the local boundary layer thickness height) for frequencies 100 kHz and 150 kHz respectively. The case for no roughness is also shown for comparison purpose. Figure 7 shows that the roughness element amplifies the perturbation at 100 kHz. Moreover, the taller the roughness element is, the stronger the amplification on the perturbation (more negative growth rate) becomes. These results are consistent with the finding in DNS that roughness amplifies perturbation lower than the synchronization frequency, and tall roughness results stronger amplification. On the other hand, for perturbation at 150 kHz shown in Figure 8, the roughness element damps the perturbation with strength depending on roughness height. It can be seen from the figure that 50% boundary layer thickness roughness element damps the perturbation significantly (growth rate is very positive). For 10% boundary layer thickness roughness element, the damping is not very significant. Again, these results are consistent with the previous DNS results as in [2, 27] which have shown roughness element can damp perturbation higher than the synchronization frequency, and the damping strength goes stronger with the roughness height goes up. Another thing that can be pointed out in Figure 7 and Figure 8 is that for the 50% local boundary layer thickness height roughness element, there is a region from x = 0.2 m to 0.22 m where PSE cannot generate any data or the PSE calculation simply blows up. The reason is because in PSE calculation, the solution in the upstream marches downstream to obtain new solutions, and around the tall roughness element, the strong flow separation region generated behind the roughness has affected the downstream region so much that it breaks down the PSE equation. The region is subsequently

recovered in the downstream region as shown in the figures, and PSE works again. For small roughness (10% local boundary layer thickness roughness), the separation is not a problem and PSE works for the whole range of interest.

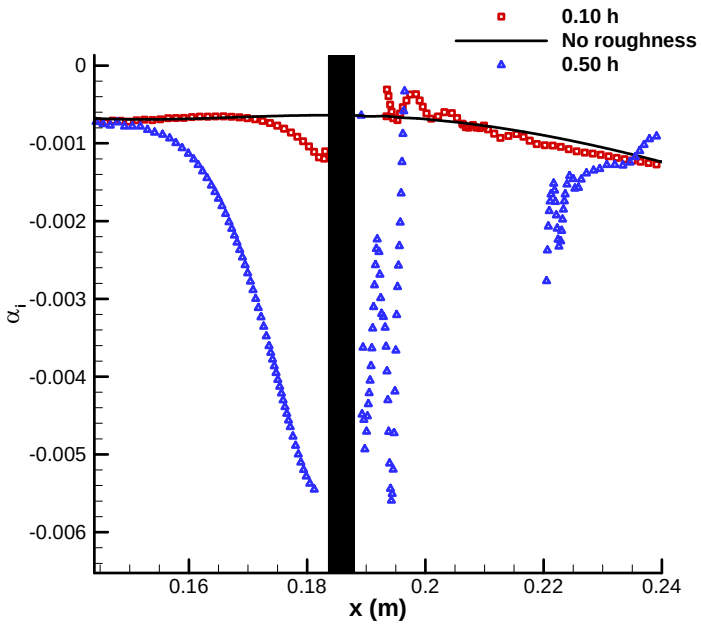

Figure 7. Growth rate obtained from PSE for 100 kHz with different roughness heights.

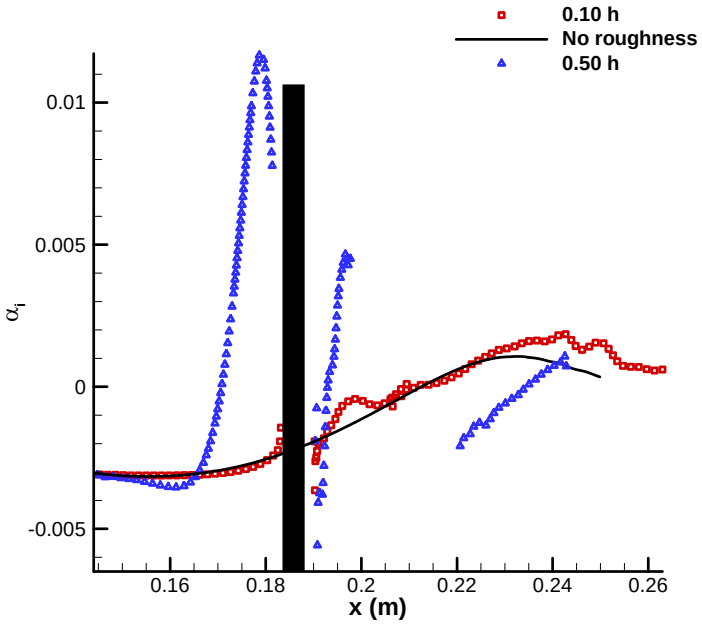

Figure 8. Growth rate obtained from PSE for 150 kHz with different roughness heights.

Other than the roughness height effect, the effect of roughness width has also been considered in the present PSE study. Figure 11 shows the schematics of pressure contour for the thin roughness and the wide roughness used here. The thin roughness has a width of 12.5% the local boundary layer thickness while the wide roughness has a width of 200% the local boundary layer thickness. Both roughness elements have a height of 50% the local boundary layer thickness. Figure 10 shows the growth rate of 100 kHz perturbation for two different roughness widths. As before,

the roughness location corresponds to the synchronization frequency of 133.26 kHz, so the roughness amplifies the perturbation of 100 kHz as shown in the figure. Although the roughness width difference is 16 times, the growth rate difference between the two roughness elements is very small. Just in front of the roughness, the difference is only about 5%. In contract, as shown in Figure 7, the roughness height difference is only 5 times, but the difference in growth rate reaches 400% just in front of roughness. This suggests that PSE predicts the sensitivity of roughness height on roughness effects is way more significant than the roughness width. This is exactly what we have shown in our previous roughness width study in [2]. The predication of PSE on roughness effects matches our DNS data once again.

In the last part of the present PSE study, it is desired to produce a contour plot of growth rate by PSE similar to the perturbation amplitude contour plot produced by DNS as shown in Figure 11, which is taken from our previous DNS study in [2]. An important feature of Figure 11 is that, on Figure 11(b) the vertical black line represents the roughness element. The horizontal line represents the synchronization location which corresponds to the roughness location. For frequencies higher than the horizontal line, their synchronization locations are upstream of the roughness, thus roughness damps those frequencies according to our DNS results. On the other hand, for frequencies lower than the horizontal line, their synchronization locations are downstream of the roughness, so roughness amplifies those perturbations at low frequencies region. The goal here is to reproduce this kind of plot using PSE analysis, but instead of pressure perturbation amplitude contour in DNS, the contour produced by PSE would be in term of growth rate. Since it has been aforementioned that a tall roughness element results discontinuity in the PSE calculation, a small roughness element of 10% the local boundary layer thickness height is used for the contour plot. Figure 12 shows the growth rate for the case without roughness element predicted by PSE. The unstable second mode waveband can be seen clearly in the figure. The case with roughness is shown in Figure 13. Same as Figure 11(b), the roughness is represented by the vertical black line, and the synchronization frequency of 133.26 kHz which corresponds to the roughness location is shown by the horizontal dash line. By comparing Figure 12 with Figure 13, it is clear that the PSE can predict the damping and amplification effects by roughness element based on the synchronization frequency. Although the effect is not significant due to the small roughness element height of 10% local boundary layer thickness used in PSE, the effect is distinguishable. Overall, PSE is shown to be capable of capturing the roughness effects observed in DNS data. Furthermore, since PSE only analyzes meanflow profiles, the fact that PSE predictions match DNS data suggests that the damping and amplification effects are the outcome of the alteration in the meanflow created by the roughness element, other than a new mode generated by the roughness element and interacts with the second mode instability waves.

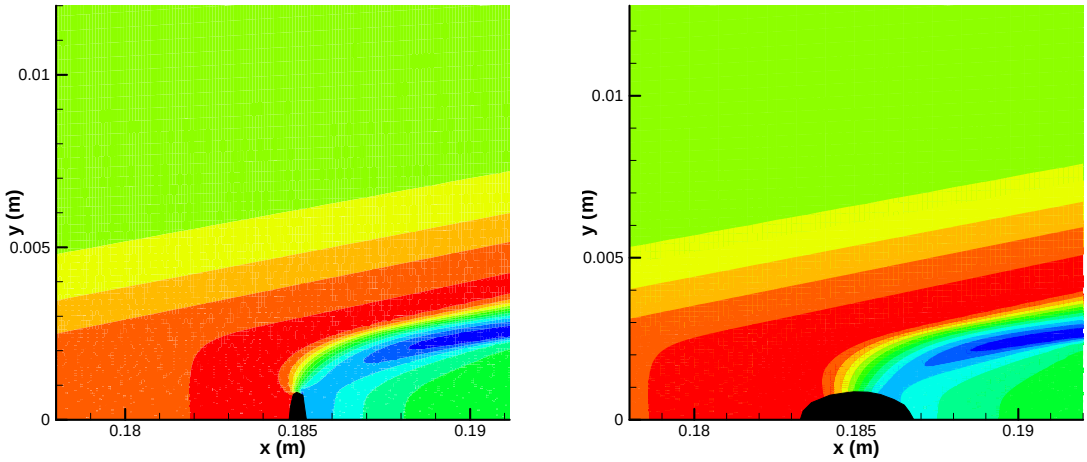

(a) 0.125 BL wide roughness (b) 2 BL wide roughness

Figure 9. Schematics of pressure contour for the thin roughness and wide roughness.

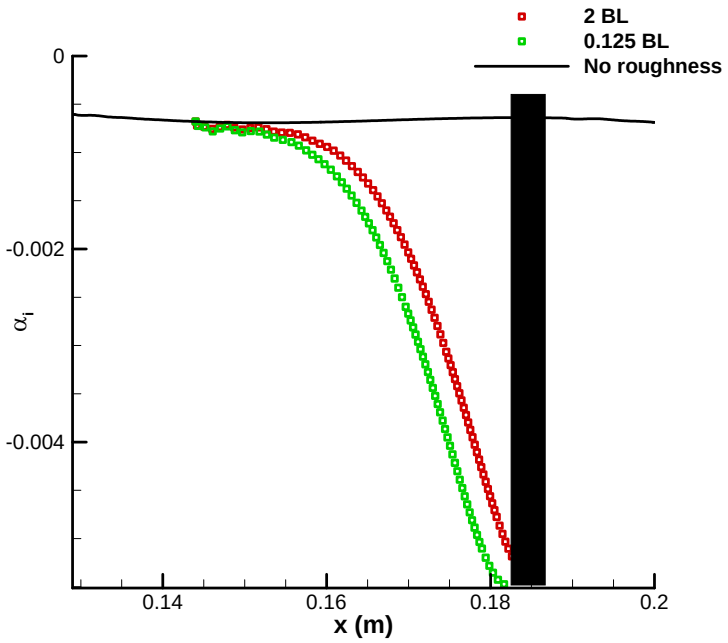

Figure 10. Growth rate obtained from PSE for 100 kHz with different roughness widths.

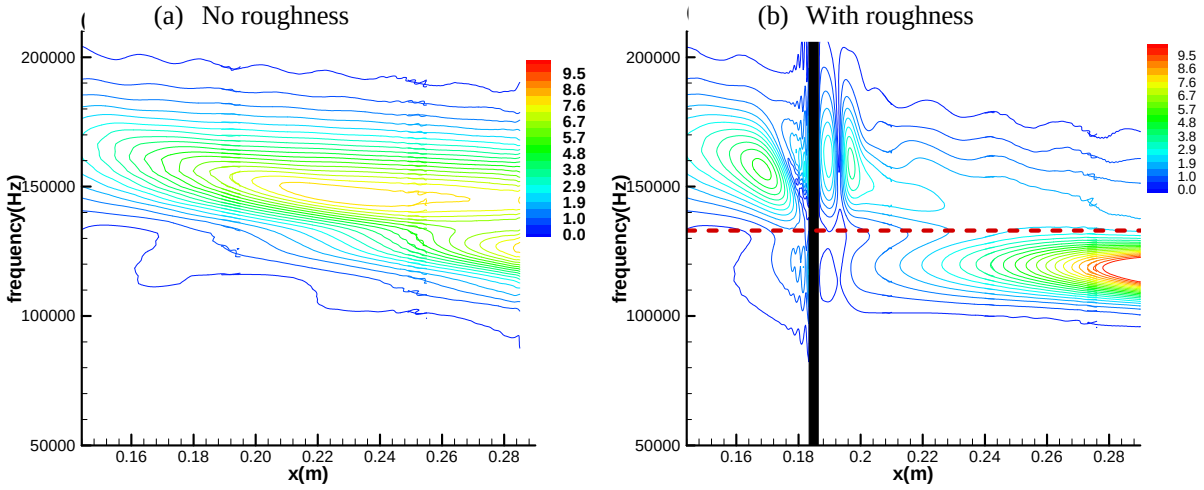

Figure 11. Perturbation amplitude contours obtained from DNS.

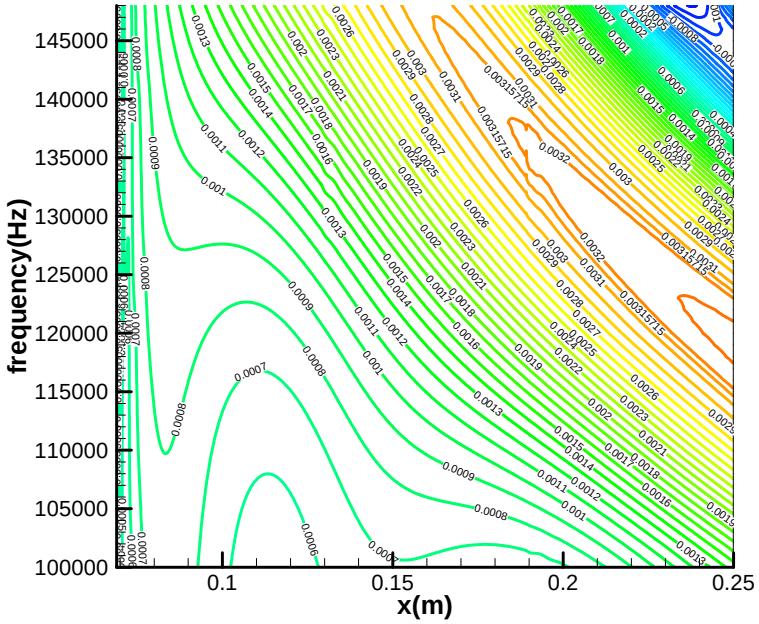

Figure 12. Growth rate contour for no roughness case by PSE.

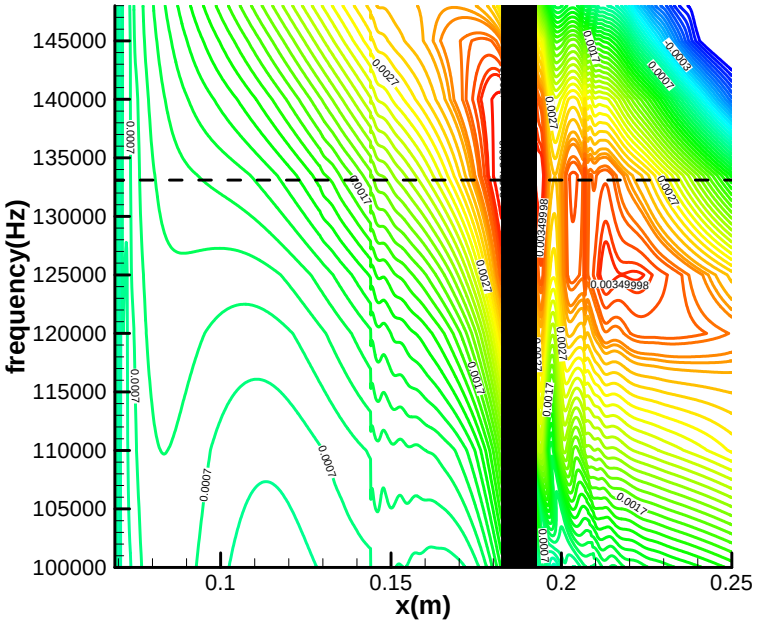

Figure 13. Growth rate contour for 10% local boundary layer thickness roughness height by PSE.

D. The Role of Synchronization Point and Neutral Point

D.1. Mach 5.92 flow with Relatively Hot Wall Condition

In this section, we investigate the role of mode S synchronization point and neutral point on roughness effect using DNS. Since the location of the neutral point and the synchronization point are usually very close to each other, it is not obvious if it is the relative location between a roughness element and synchronization point that is important, or it is actually the relative location between a roughness element and neutral point that plays an important role. To address this question, we have looked at the location of the mode S neutral point and also the synchronization point in our most studied flow condition, which is as follow:

$$\begin{cases} P_r = 0.72, R_\infty = \rho_\infty u_\infty / \mu_\infty = 13.2\times 10^6 / m \\ M_\infty = 5.92, T_\infty = 48.69K, P_\infty = 742.76Pa, T_w = 334.9K \end{cases}$$

The detail of stability analysis on this flow condition has been done in [37]. It shows the location of neutral point and synchronization point for different frequencies. In particular, Figure 14 shows the phase velocity and growth rate are self-similar for two different locations on the flat plate. It is found from Figure 14 that the branch I neutral point locates at $\omega_I = 0.00827$ and the synchronization point is at $\omega_s = 0.11563$. Using the definition of dimensionless frequency of $\omega = F\sqrt{x\,\mathrm{Re}_\infty}$, the physical locations of the neutral point x_1 and the synchronization point x_s for frequencies of 100 kHz and 150 kHz are found to be as follow:

$$x_1 = 1.69744\times 10^{-3}\ \text{m}\ ,\ x_s = 0.33184\ \text{m}\ \ \text{for 100 kHz}$$
$$x_1 = 7.54418\times 10^{-4}\ \text{m}\ ,\ x_s = 0.14748\ \text{m}\ \ \text{for 150 kHz}$$

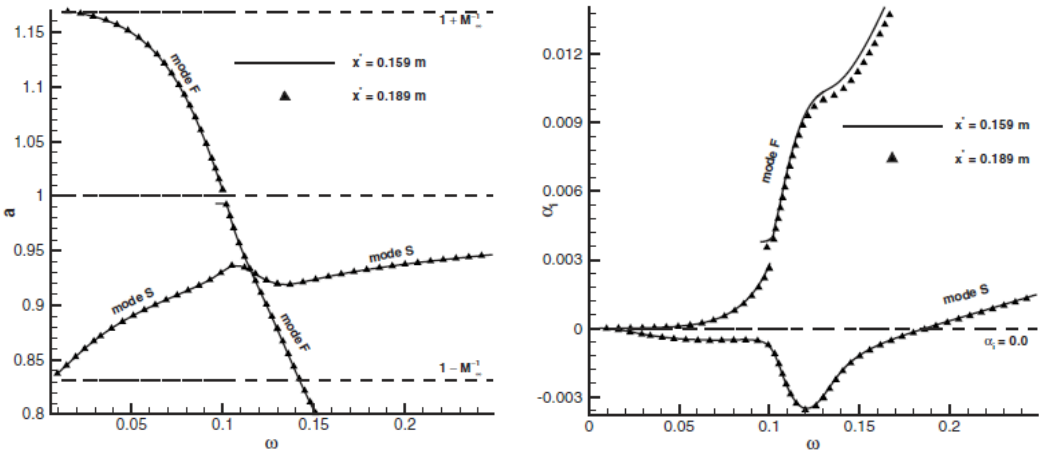

Figure 14. Distributions of phase velocity and growth rates of modes F and S at two different locations.

It can be seen that in this flow condition, mode S becomes unstable at the very early stage (the first mode stage), thus the neutral point is way upstream compared with the synchronization location. As a result, the roughness locations of the cases that we have tested are effectively way behind the neutral points. However, the role of synchronization point can be unmistakably seen for this flow condition from our DNS results. In the previous section, Figure 2 has shown the frequency spectrum for different locations downstream of the roughness, it can be clearly seen that the frequencies higher than the synchronization frequency of have been strongly damped by the roughness, and for frequencies lower than 133.26 kHz have been amplified. Since the location of synchronization point is frequency dependent, for frequencies higher than the synchronization frequency, their synchronization points are more upstream. It means that the roughness is downstream of their synchronization point. Vice versa, for frequencies lower than the synchronization frequency, their synchronization points are more downstream. As a result, the roughness element is upstream of their synchronization points. The role of synchronization point is obvious. The same conclusion can also be drawn from Figure 11 (b). The frequencies higher than the horizontal line,

which is higher than the frequency of 133.26 kHz has been damped, while those lower than the horizontal line, which is lower than 133.26 kHz, have been amplified.

The role of synchronization point also manifests itself once again in our previous parametric study of roughness effect [2]. Figure 15 shows the perturbation amplitude contours obtained from FFT, which is similar to Figure 11 and Figure 13. But here, it is for a multiple roughness elements case. The two vertical black lines represent the locations of the two roughness elements. The horizontal red dash lines represent the synchronization frequencies at which the roughness elements are located. For example, in Figure 15 (a), the first roughness is at 0.185 m. This location is the synchronization point of 133.26 kHz perturbation, which is represented by the top red dash line. The second roughness location, 0.25 m, is the synchronization point of perturbation at frequency 115 kHz which is represented by the lower red dash line. One important feature in Figure 15 which should be clarified is the following: for frequencies higher than the upper red dash line, both the first and the second roughness elements are downstream of their synchronization points. And as shown in the figure, those frequencies are damped by both roughness elements. On the other hand, for frequencies between the two dash lines, the first roughness is upstream of their synchronization points while the second roughness is downstream of their synchronization points. It is shown in the figure that the first roughness amplifies those frequencies while they are damped by the second roughness. Lastly, both roughness elements are upstream of the synchronization points for the frequencies below the lower red dash line, and it is shown that those frequencies are amplified by the two roughness elements. Figure 16 shows a clearer picture by showing the spatial growth of two selected frequencies of 120 kHz and 140 kHz. The 120 kHz perturbation is between the two horizontal lines in Figure 15. As a result, the perturbation is amplified by the first roughness while it is damped by the second roughness. On the other hand, 140 kHz perturbation is above top horizontal line. Therefore, it is strongly damped by both roughness elements.

In conclusion, the role of the synchronization point in roughness effect is overwhelmingly obvious judging from our DNS simulation, even for a flow condition in which the neutral point is way upstream of the roughness elements.

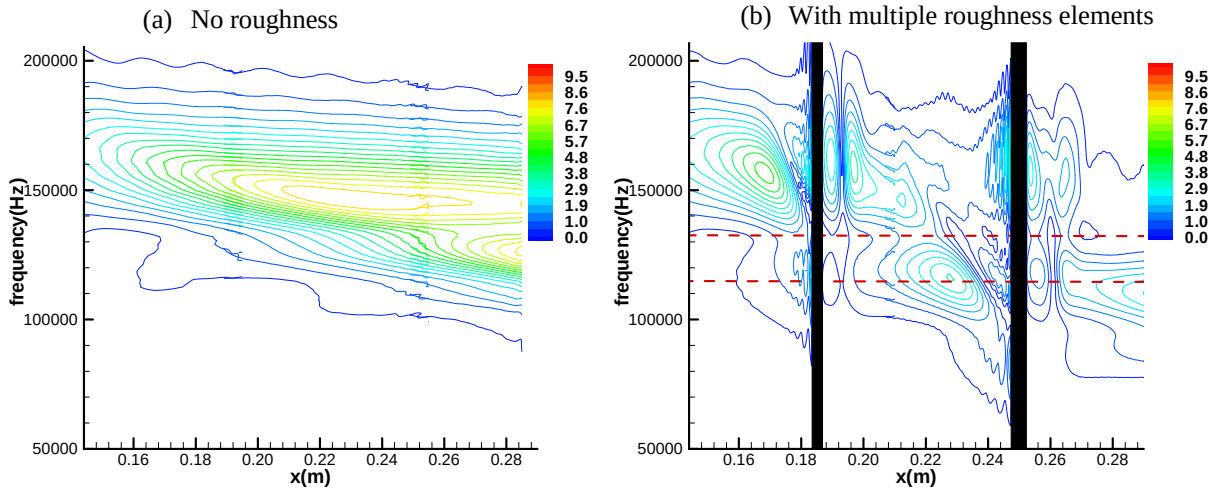

Figure 15. Perturbation amplitude contours obtained from FFT for multiple roughness elements.

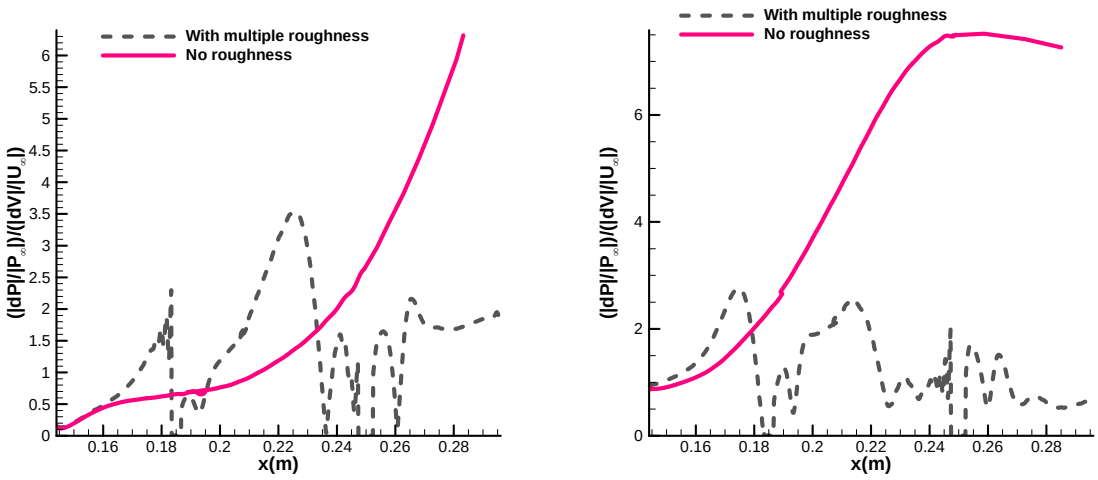

(a) 120 kHz (b) 140 kHz

Figure 16. Spatial growth of different selected frequencies for multiple roughness elements case.

D.2. Mach 5.92 flow with relative cold wall condition

Since the neutral point in the previous flow condition is far upstream, we have simulated another case where the neutral point and synchronization point are closer together. To achieve this, a meanflow of the same freestream conditions but with a colder wall temperature (from $T_w = 350\text{K}$ to $T_w = 155.6\text{K}$) is computed by DNS. It is well known that cold wall temperature stabilizes first mode, while it destabilizes the second mode. Lowering the wall temperature effectively moves the mode S neutral point downstream closer to the synchronization point as the first mode is stabilized. Figure 18 shows the phase velocity and growth rate for the cold wall case similar to Figure 14. As it can been seen from Figure 18 (a) and (b), the mode S neutral point is around $\omega_I = 0.121$, and the synchronization point is around $\omega_s = 0.136$. On the other hand, we have placed the roughness in this meanflow at the same location as previously at $x = 0.185$ m as shown in Figure 17, and the roughness height is fixed at 50% local boundary layer thickness. With these information, the roughness location are found to be corresponding to the neutral point for frequency of 139 kHz, and the synchronization point of frequency 152 kHz. Figure 19 shows the spatial growth of perturbation with and without roughness for different frequencies of 130 kHz, 135 kHz, 140 kHz, 145 kHz, 150 kHz and 155 kHz obtained from DNS. In Figure 19 (a) and (b) for 130 kHz and 135 kHz perturbations, the roughness is upstream of both the neutral point and the synchronization point. We can see that roughness amplifies these two frequencies of perturbations significantly. On the other hand, in Figure 19 (c), since the neutral point for 139 kHz is located at the roughness location of $x = 0.185$ m, we can clearly see that the perturbation of 140 kHz (which is close to 139 kHz) starts to grow exponentially around $x = 0.185$ m without roughness. If a roughness element is placed at $x = 0.185$ m, it is seen that the roughness still amplify the perturbation even the roughness is located very close to its neutral point. On the other hand, the perturbation of 145 kHz is also amplified by the roughness with it being downstream of its neutral point. However, the trend is reversed when roughness is close to the synchronization point. As shown in Figure 19 (e), the roughness element starts to damp the perturbation as the roughness element gets very close the synchronization of 150 kHz perturbation. The damping effect becomes even stronger for perturbations at higher frequency as in Figure 19 (f), where the roughness is way behind the synchronization location of 155 kHz.

Figure 20 shows the pressure perturbation amplitude contour for the cold wall case similar to Figure 11. Figure 20 (a) is the case without roughness while Figure 20 (b) shows the case with roughness. As before, the vertical black line in Figure 20 (b) presents the roughness element. But here, two horizontal black lines are shown: the lower horizontal black line presents the neutral frequency (139 kHz) corresponding to the roughness location, while the upper horizontal black line presents the synchronization frequency (152 kHz). From the figure, it is clear that the frequencies below the synchronization frequency are strongly amplified by the roughness. On the other hand, the frequencies higher than synchronization frequency are strongly damped by the roughness. Our DNS results have

shown that the location of neutral point has minimal effect on roughness effects of damping/amplification perturbations. It is the relative location of the synchronization location and the roughness location that plays the important role in the roughness effects.

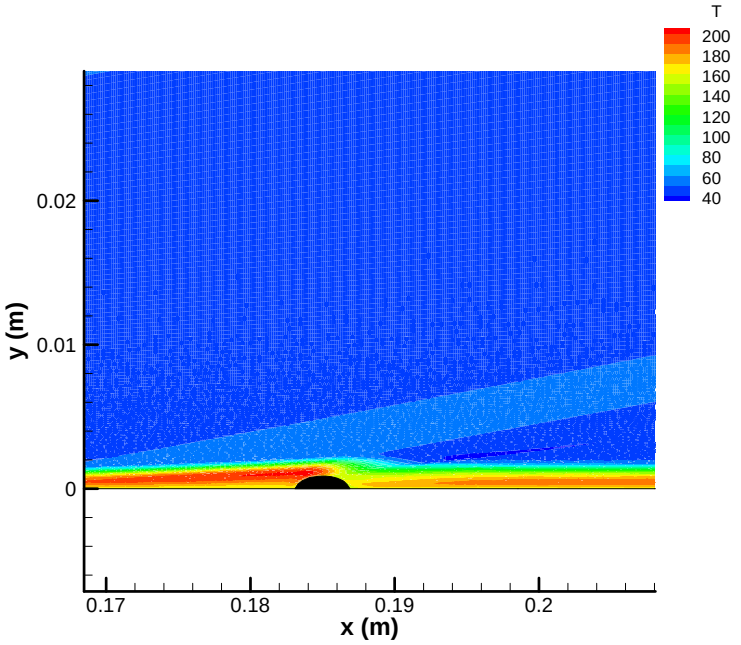

Figure 17. Temperature contour with roughness element for the cold wall test case.

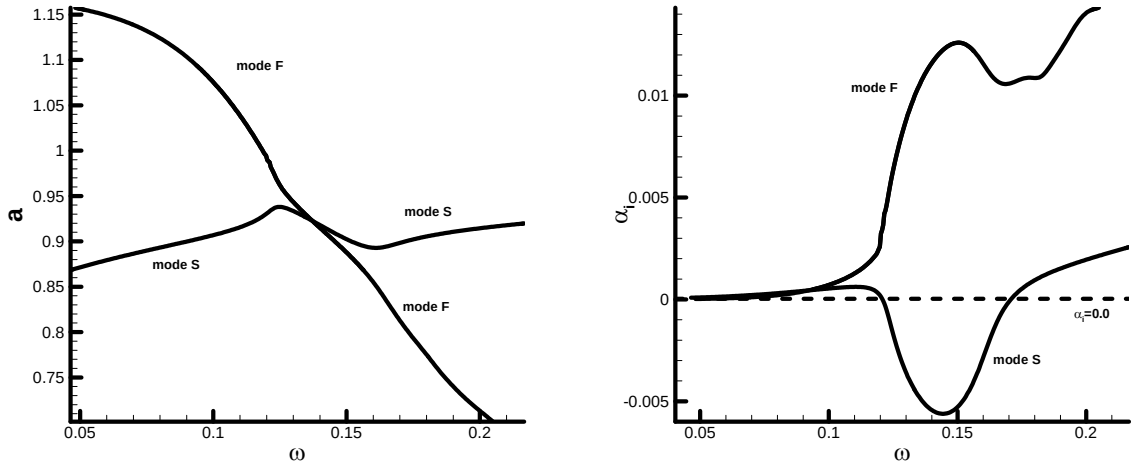

Figure 18. Distributions of phase velocity and growth rates of modes F and S at two different locations for the cold wall case.

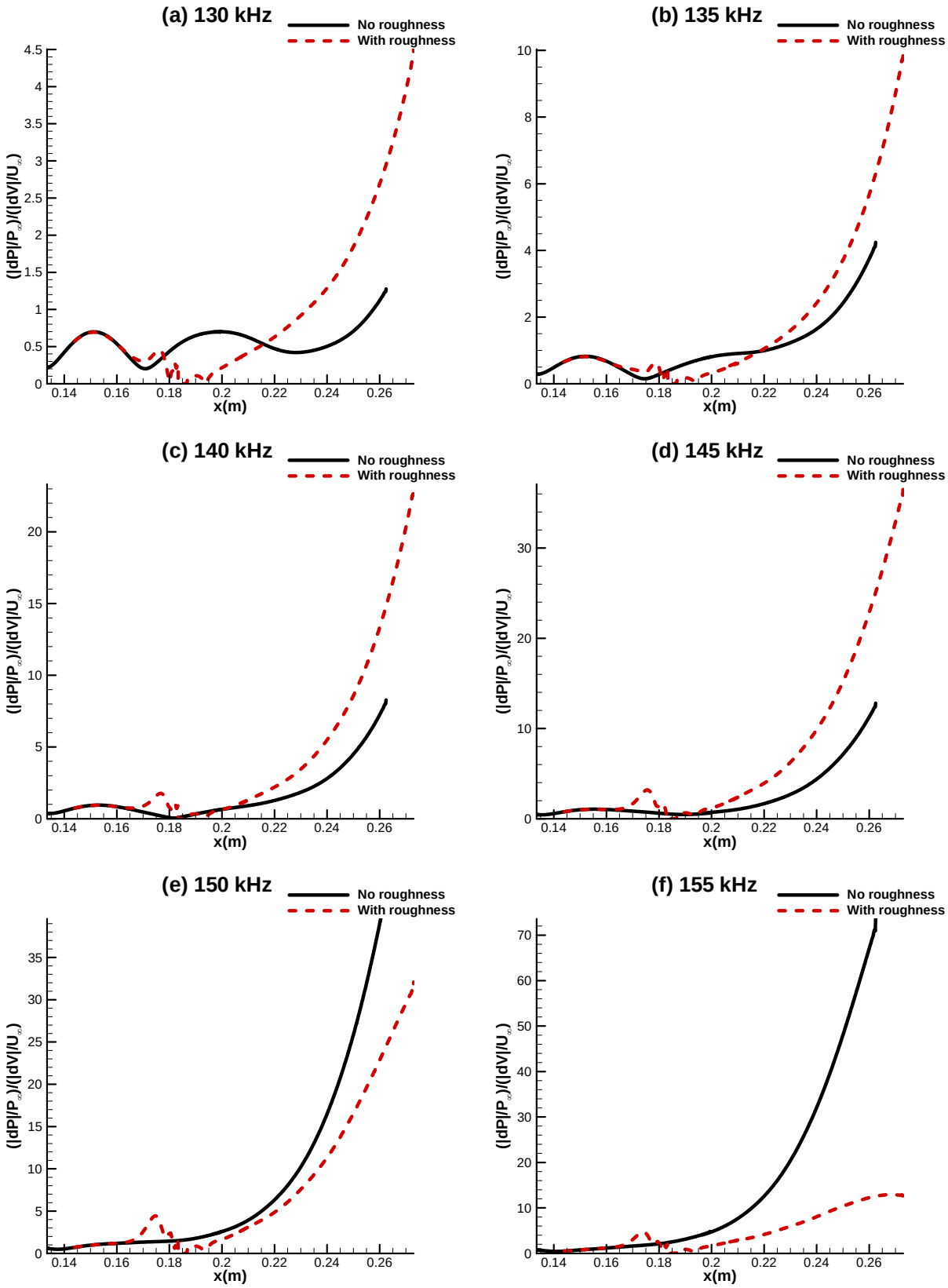

Figure 19. Spatial growth of different frequencies with and without roughness element on the cold wall case.

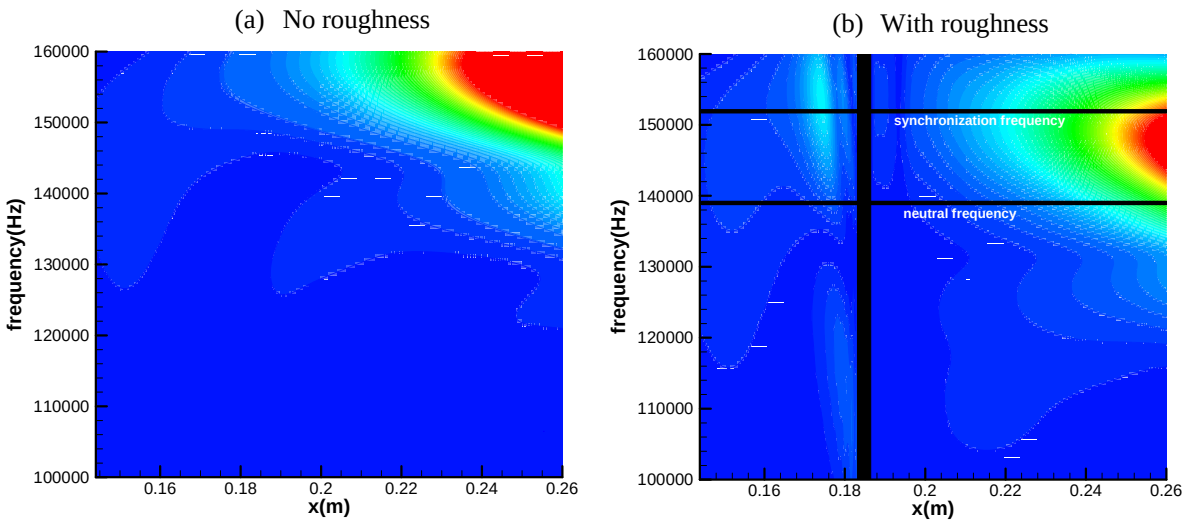

Figure 20. Perturbation amplitude contours obtained from DNS for the cold wall case.

V. Summary

In this paper, DNS and PSE analysis have been performed on a hypersonic boundary layer flow with and without roughness elements with different heights and widths. The goal of this study is to investigate the mechanism of roughness effects using DNS and the theoretical approach of PSE. The results of PSE are then compared with the results in our previous DNS studies [1, 2, 27, 29, 35, 36], which show roughness elements damp mode S perturbation if the roughness are placed downstream of the synchronization point, and amplify the mode S perturbation if the roughness are placed upstream of the synchronization point. The PSE code is shown to be reduced to LST successfully by assuming parallel flow for validation purpose. Then, the PSE code is used for different mean flows with roughness element. Our results have shown that PSE is capable of accurately predicting the roughness effects observed in DNS data. For instance, our PSE has shown that the relative location of the roughness and the synchronization frequency is important, which confirms our observation from simulations. On the other hand, our PSE results show that a tall roughness gives a stronger amplification/damping effect on the mode S perturbation and the roughness width effect is insignificant compared with the roughness height. These two trends match our previous conclusion about roughness height and width from the DNS data as in [2]. Since PSE only analyzes the steady meanflow with roughness element, the accurate prediction from PSE means that the stabilization/amplification effects are not generated by a new mode. Rather, the roughness effects are created by the meanflow alterations by the roughness element.

Finally, we have investigated the role of neutral point and the synchronization point by DNS. Our simulations show overwhelmingly the synchronization point is important on the roughness effect even for a meanflow where the neutral point is far upstream. On the other hand, by computing a new meanflow with lower wall temperature, we can distinguish the two points within a reasonable distance. Our results show the neutral point plays a minimal role in determining the roughness effects on the mode S perturbation. On the contrary, the relation of the location of synchronization point and roughness effect is obvious and important.

Acknowledgments

This work was sponsored by the Air Force Office of Scientific Research, USAF, under AFOSR Grants #FA9550-15-1-0268, first monitored by Dr. Rengasamy Ponnappan, and now by Dr. Ivett Leyva. The computations are mainly run on XSEDE resources provided by TACC under grant number TG-ASC090076 supported by National Science Foundation. The views and conclusions contained herein are those of the author and should not be interpreted as necessarily representing the official policies or endorsements either expressed or implied, of the Air Force Office of Scientific Research or the U.S. Government.

References

1. Fong, K.D., Wang, X., Huang, Y., Zhong, X., Mckieman, G.R., Fisher, R.A., and Schneider, S.P., *Second Mode Suppression in Hypersonic Boundary Layer by Roughness: Design and Experiments.* AIAA JOURNAL, 2015. **53**(10): p. 3138-3144.
2. Fong, K.D., Wang, X., and Zhong, X., *Parametric Study on Stabilization of Hypersonic Boundary-Layer Waves Using 2-D Surface Roughness.* AIAA paper, 2015. **2015-0837**.
3. Board, D.S., *Final report of the second defense science board task force on the national aero-space plane (NASP).* 1992. p. 94-00052.
4. Anderson, J.D., *Hypersonic and high temperature gas dynamics*. 2000: AIAA.
5. Berry, S., Horvath, T., *Discrete roughness transition for hypersonic flight vehicles*, in *45th AIAA Aerospace Sciences Meeting and Exhibit*. 2007: Reno, Nevada.
6. Saric, W.S., Reed, H. L., and Kerschen, E. J., *Boundary-Layer Receptivity to Freestream Disturbances.* Annual Review of Fluid Mechanics, 2002. **34**: p. 291-319.
7. Mack, L.M., *Boundary layer linear stability theory*, in *AGARD Report*. 1984. p. 1-81.
8. Maslov, A.A., Shiplyuk, A. N., Sidorenko, A., and Arnal, D., *Leading-edge Receptivity of a Hypersonic Boundary Layer on a Flat Plate.* Journal of Fluid Mechanics, 2001. **426**: p. 73-94.
9. Maslov, A.A., Mironov, S. G., Shiplyuuk, A. A., Sidorenko, A. A., Buntin, D. A., and Aniskin, V. M., *Hypersonic Flow Stability Experiments.* 2002. **AIAA 2002-0153**.
10. Demetriades, A., *Hypersonic Viscous Flow Over A Slander Cone. Part III: Laminar Instability and Transition.* AIAA paper 74-535, 1974.
11. Demetriades, A., *Laminar Boundary Layer Stability Measurements at Mach 7 Including Wall Temperature Effects.* AFOSR-TR-77-1311, 1977.
12. Malik, M.R., Lin, R. S., and Sengupta, R., *Computation of Hypersonic Boundary-Layer Response to External Disturbances.* AIAA paper 1999-0411, 1999.
13. Ma, Y., and Zhong, X., *Receptivity to Freestream Disturbances of Mach 8 Flow over A Sharp Wedge.* AIAA paper 2003-0788, 2003.
14. Wang, X., Zhong, X., and Ma, Y., *Response of a hypersonic boundary layer to wall blowing - suction.* AIAA Journal, 2011. **In press**.
15. Balakumar, P. *Transition In a Supersonic Boundary-Layer Due To Roughness Aand Acoustic Disturbances*. in *AIAA*. 2003.
16. Marxen, O., Iaccarino, G., *Numerical simulation of the effect of a roughness element on high-speed boundary-layer instability*, in *38th Fluid Dynamics Conference and Exhibit*. 2008: Seattle, Washington.
17. Marxen, O., Iaccarino, G. and Shaqfeh,E.S.G., *Disturbance evolution in a Mach 4.8 boundary layer with two-dimensional roughness-induced separation and shock.* Journal of Fluid Mechanics, 2010. **648**: p. 435-469.
18. Duan, L., Wang, X., and Zhong, X. , *A high-order cut-cell method for numerical simulation of hypersonic boundary-layer instability with surface roughness.* Journal of Computational Physics, 2010. **229**(19): p. 7207-7237.
19. Riley, Z.B., McNamara J.J. and Johnson, H.B., *Hypersonic Boundary Layer Stability in the Presence of Thermo-Mechanical Surface Compliance*, in *AIAA Paper 2012-1549*. 2012.
20. Riley, Z.B., McNamara J.J. and Johnson, H.B., *Assessing Hypersonic Boundary-Layer Stability in the Presence of Structural Deformation.* AIAA Journal, 2014. **DOI: 10.2514/1.J052941**.
21. Egorov, I.V., Novikov, A.V., and Fedorov, A. V. *Direct numerical simulation of supersonic boundary layer stabilization using grooved wavy surface*. in *AIAA paper 2010-1245*. 2010.
22. Balakumar, P., *Stability of Hypersonic Boundary-Layers over a Compression Corner*, in *AIAA Paper 2002-2848*. 2002.
23. Egorov, I.V., Fedorov, A. V., and Novikov, A.V., *Numerical Modeling of the Disturbances of the Separated Flow in a Rounded Compression Corner.* Fluid Dynamics, 2006. **41**(4): p. 521-530.
24. Bountin, D., Chimitov, T., Maslov, A.,Novikov, A.,Egorov, I.,Fedorov,A.,Utyuzhnikov,S., *Stabilization of Hypersonic Boundary Layer Using a Wavy Surface.* AIAA Journal, 2013. **51**(5): p. 1203-1210.
25. Duan, L., Wang, X., and Zhong, X., *A High-Order Cut-Cell Method for Numerical Simulation of Hypersonic-Boundary Transition with Arbitrary Surface Roughness.* AIAA paper 2009-1337, 2009.
26. Fujii, K., *Experiment of the Two-Dimensional Roughness Effect on Hypersonic Boundary-Layer Transition.* Journal of Spacecraft and Rockets, 2006. **43**(4): p. 731-738.
27. Fong, K.D., Wang, X, and Zhong, X, *Numerical simulation of roughness effect on the stability of a hypersonic boundary layer*. Computers and Fluids, 2014. **96**: p. 350-367.
28. Fong, K.D., Wang, X., and Zhong, X., *Parametric Study on Stabilization of Hypersonic Boundary-Layer Waves Using 2-D Surface Roughness.* AIAA Paper 2015-0837, 2015.
29. Fong, K., Wang, X. and Zhong, X., *Stabilization of Hypersonic Boundary Layer by 2-D Surface Roughness.* AIAA paper, 2013. **2013-2985**.
30. Gao, B., and Park, S.O. *Compressible Parabolized Stability Equation in Curvilinear Coordinate System and Integration*. in *KSAS International Journal*. 2006.
31. Chang, C.L., Malik, Muheeb R., Erlebacher, G. and Hussaini M.Y., *Linear and Nonlinear PSE for Compressible Boundary Layer*. 1993, NASA Report.

32. Park, D., and Park, S.O., *Study on Stabilization and Destabilization Effect of a Smooth Hump in Hypersonic Boundary Layer by PSE*. AIAA paper 2013-2742, 2013.
33. Malik, M.R., *Hypersonic Flight Transition Data Analysis Using Parabolized Stability Equations with Chemistry Effects*. Journal of Spacecraft and Rockets, 2003. **40**(3): p. 332-344.
34. Fong, K.D., Wang, X., and Zhong, X., *Numerical Simulation of Roughness Effect on the Stability of a Hypersonic Boundary Layer*. Seventh International Conference on Computational Fluid Dynamics (ICCFD7), 2011. **ICCFD7-1502**.
35. Fong, K., Wang, X. and Zhong, X., *Finite roughness effect on modal growth of a hypersonic boundary layer*, in *50th AIAA Aerospace Sciences Meeting Including the New Horizons Forum and Aerospace Exposition*. 2012: Nashville, Tennessee, USA.
36. Fong, K.D., Wang, X., and Zhong, X., *Numerical Simulation of Roughness Effect on the Stability of a Hypersonic Boundary Layer*. ICCFD7-1502, 2012.
37. Wang, X., and Zhong, X., *Effect of wall perturbations on the receptivity of a hypersonic boundary layer*. Physics of fluids, 2009. **21** (044101).